

## Influence of The KF Concentration on The Coating Process And Properties of Potentiostatic Deposited Fluoride Conversion Film on AZ31 Mg Alloy

Liping Wu, Lin Zhao, Junhua Dong\*, Wei Ke, Xiaofang Li  
Environmental Corrosion center, Institute of Metal Research, Chinese Academy of Sciences,  
Shenyang, 110016, China

### Research Article

Received date: 22/04/2015  
Accepted date: 22/05/2015  
Published date: 27/05/2015

#### \*For Correspondence

Junhua Dong, Tel: +86 24 23915912; Fax: +86  
24 23894149

E-mail: jhdong@imr.ac.cn

**Keywords:** Fluoride conversion film, AZ31 magnesium alloy, KF solutions, Potentiostatic deposition.

#### ABSTRACT

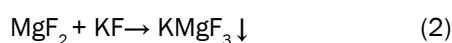
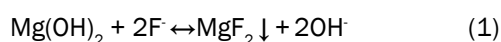
The dependence of coating process and properties of the fluoride conversion film on AZ31 Mg alloy on the concentration of deaerated KF solutions was studied by anodic potentiostatic deposition, scanning electron microscopy (SEM), energy dispersive X-ray spectroscopy (EDS), X-ray diffraction (XRD), X-ray photoelectron spectroscopy (XPS), and electrochemical impedance spectroscopy (EIS). The results show that the film deposited in 0.05 M KF solution is a monolayer consisting of amorphous  $\text{Mg}(\text{OH})_2$  and  $\text{MgF}_2$ , while amorphous  $\text{Mg}(\text{OH})_2$  and  $\text{MgF}_2$  and crystallized  $\text{KMgF}_3$  as a double layer formed in 0.1 M~0.5 M KF solutions. The composition of inner layer is same as that of the monolayer, while the outer layer is composed of  $\text{Mg}(\text{OH})_2$  and  $\text{MgF}_2$  and  $\text{KMgF}_3$ . Continually increasing KF concentration reduces the content of  $\text{KMgF}_3$  in the outer layer, shortens the coating duration, and reduces the film thickness. The corrosion resistance of FCF coatings is closely correlated with the content of  $\text{KMgF}_3$  and the film thickness.

### INTRODUCTION

Magnesium (Mg) and its alloy have closer density and elastic modulus (density: 1.7–2.04 g/cm<sup>3</sup>, Young's modulus: 41–45 GPa) to those of natural bone (density: 1.8–2.1 g/cm<sup>3</sup>, Young's modulus: 10–30 GPa) than traditional implants such as 316L stainless steels, Ti6Al4V alloys, Co-Cr based alloys, thus when implanted they can minimize the stress shielding effect that can cause delay in healing process of damaged bones and implant loosening<sup>[1-3]</sup>. Additionally, Mg can be excreted in terms of soluble  $\text{MgCl}_2$  through urine, and Mg is considered as a beneficial element in maintaining the normal function of the human metabolism and the growth of new bone tissue<sup>[2,3]</sup>. Moreover, Mg can totally degrade in the physiological system (pH 7.4-7.6), thus eliminating the need for secondary surgery<sup>[4-5]</sup>. These intriguing characteristics make Mg and its alloys have great potential in orthopaedic application. Nevertheless, most of currently developed high purity Mg and Mg alloys fail only within 1~2 months in the human body fluids<sup>[4]</sup>, while damaged bones need at least 3 months to heal<sup>[4]</sup>, thus negatively affecting the bone tissue regeneration. Meanwhile, the generation of subcutaneous hydrogen gas ( $\text{H}_2$ ) and the accumulation of bubbles in gas pockets adjacent to the implant will occur during their degradation. If the volume of accumulated  $\text{H}_2$  reaches a high level, it will cause separation of tissue and tissue layers<sup>[4-7]</sup>. Consequently, in order to decrease their degradation rate and thus accumulation of  $\text{H}_2$  to match the healing rate of damaged bones, fluoride conversion film (FCF) has been developed, attributed to the harmlessness of the fluorine ions releasing into the organism<sup>[8]</sup>, its good biotissue compatibility<sup>[9-12]</sup>, excellent cell adhesion<sup>[13-14]</sup>, and its characteristics to accelerate the osseointegration rate<sup>[15]</sup>, enhance bone healing<sup>[16]</sup> and prevent the biofilm formation<sup>[17-19]</sup>. The original method to fabricate FCF on Mg substrate was immersion of Mg substrate in 40% or 48% hydrofluoric acid, HF<sup>[19-25]</sup>, however, the high toxicity

and volatility associated with HF has pushed the development of fluoride films in KF solution due to its low cost, non-toxicity and easiness for biomedical applications.

Pereda et al. [26, 27] firstly carried out the potentiostatic deposition of FCF on pure Mg in KF solution. They found the effect of KF concentration on the corrosion resistance of FCF coated pure Mg. They reported that the best corrosion resistant FCF coating on pure Mg was formed in 0.1 M KF solution, and the potassium magnesium fluoride,  $\text{KMgF}_3$  is one of the main constitute in the film. However, the FCF coating formed in 1 M KF solution was poor of corrosion resistance and  $\text{MgF}_2$  was observed as a main composition in the film. Sankara Narayanan et al [28] improved the corrosion resistance of FCF coated pure Mg by adding  $\text{K}_2\text{CO}_3$  in 48% HF via the formation of  $\text{KMgF}_3$ , and they suggested that the film with higher F/O ratio or higher content of  $\text{MgF}_2$  should correspond to the better corrosion protective ability, which was also demonstrated by Chiu et al [29]. Moreover, Wu et al [30] suggested a coating process of FCF deposited on AZ31 Mg alloy in the deaerated 0.1 M KF solution with pH 7.5 at  $-1.4$  V, in which the initial corrosion product was composed of  $\text{Mg}(\text{OH})_2$ , then it was transformed to  $\text{MgF}_2$  under the attack of F<sup>-</sup>; and finally some of the formed  $\text{MgF}_2$  combined with KF to form  $\text{KMgF}_3$ . It has been demonstrated that the FCF coating is composed of  $\text{Mg}(\text{OH})_2$ ,  $\text{MgF}_2$  and  $\text{KMgF}_3$ . The chemical reaction for forming  $\text{MgF}_2$  and  $\text{KMgF}_3$  can be shown as formulas (1) and (2), respectively. Clearly, increasing the concentration of F<sup>-</sup> or decreasing the pH of the solution should shift the equilibrium of formula (1) from  $\text{Mg}(\text{OH})_2$  to  $\text{MgF}_2$ , and thus it also should be in favor of producing more precipitate of  $\text{KMgF}_3$  according to formula (2).



However, as Pereda et al. [26,27] pointed out, the higher concentration of KF solution did not bring the better corrosion resistant FCF coating and much more precipitate of  $\text{KMgF}_3$ . So far, this is still an unknown fact that needs to clarify.

In the present study, the effect of the KF concentration on the chemical composition, structure and corrosion resistance of the potentiostatic deposited FCF coating were systematically studied by the methods of potentiostatic deposition, cyclic voltammetry, XPS, XRD, SEM, EDS, and EIS. The explanation for the difference of FCF coatings formed in the solutions with different KF concentrations was proposed.

## EXPERIMENT

### Potentiostatic polarization of sample

AZ31 magnesium alloy specimens (composition (in wt %): 2.98 Al, 0.88 Zn, 0.38 Mn, 0.0135 Si, 0.001 Cu, 0.002 Ni, 0.0027 Fe and balance Mg) with a dimension of 20 mm × 15 mm × 4 mm were mechanically ground with silicon carbide (SiC) paper to 5000 grit, then it was ultrasonically cleaned in ethanol, subsequently it was dried in a cold air stream. The specimen was then welded to an electrical wire, followed by sealed into 704 RTV silicone with about 1 cm<sup>2</sup> of exposed surface area. After 5 min drying in air, the encapsulated specimen was then immersed in a standard three-electrode cell containing aqueous KF solutions which were prepared by dissolving analytical grade KF salts in deionized water. The working electrode was the encapsulated specimen, the counter electrode was a platinum electrode and the reference electrode, to which all potentials are referred, was a saturated calomel electrode. After the solution was deaerated with nitrogen ( $\text{N}_2$ ) for 1 h, the specimen was immersed in the solution, followed by immediate potentiostatic polarization at  $-1.4$  V with a Potentiostat/Galvanostat 273A at room temperature of 25 °C.

### Cyclic voltammetry tests

The encapsulated AZ31 Mg alloy electrodes were investigated using cyclic voltammetry (CV) with Gamry electrochemical workstation (Reference 6000 Potentiostat/Galvanostat/ZRA) in deaerated KF solution of pH 7.5. The electrode was cycled from  $-1.5$  V to  $-1.0$  V, and followed by reverse scan from  $-1.0$  V to  $-1.5$  V at a scan rate of 150 mV/s.

### Film characterization

The surface morphology of the FCF was examined with a Phillips FEI INSPECTF Scanning Electron Microscopy (SEM), while its cross section morphology was identified with a Phillips XL30 Environmental Scanning Electron Microscopy (ESEM). Both FEI INSPECTF SEM and ESEM were equipped with Energy Dispersive X-ray analysis (EDS).

The crystallographic structure of FCF on AZ31 alloy was characterized by a Philips PW1700 X'Pert X-ray generator using  $\text{Cu K}\alpha$  radiation in a range of  $20^\circ \sim 90^\circ$  with a step size of  $0.04^\circ$  at time per step of 0.8 s.

The surface chemical composition and elemental depth profiles of FCF was analyzed by X-ray photoelectron spectroscopy (XPS). Photoelectron spectra were obtained with a Thermo VG ESCALAB 250 spectrometer equipped with a monochromated Al  $\text{K}\alpha$  X-ray source (incident energy of 1486.6 eV, pass energy of 50 eV) powered at 150 W, calibrated relative to the C 1s peak at 284.6 eV. During elemental depth profiling, samples were etched by ionized argon in the preparation chamber at a vacuum of  $6 \times 10^{-8}$  mbar with an etching rate of 0.2 nm/s. The measured sample current was 2  $\mu\text{A}$  with a bombardment area of 2 mm × 2 mm.

Electrochemical impedance spectroscopy (EIS) test was carried out using a Potentiostat/Galvanostat 273A at room temperature in 0.1 M NaCl aqueous solution in the same cell with that used for the potentiostatic polarization, and it was started immediately after immersion of the coated specimen in 0.1 M NaCl solution. The EIS analyses were carried out using a Signal

Recovery Model 5210 lock in amplifier in a frequency range from  $10^5$  to 0.01 Hz with an applied 5 mV sinusoidal perturbation. All spectra were recorded at open circuit potential, and 51 experimental data points were collected during the measurements. EIS data were fitted with ZSimpWin3.10 software.

## RESULTS AND DISCUSSION

### Potentiostatic deposition process of FCF

Figure 1 shows the potentiostatic current decay curves of AZ31 Mg alloy obtained at  $-1.4$  V vs SCE in the deaerated KF solution with different concentrations and pH 7.5. In general, all of the current decay curves can be divided into three stages, in which the first stage (S1) corresponds to the sum of the charging process of the electric double layer and electrode reactions, the second stage (S2) describes to the coating process of FCF layer, and finally in the third stage (S3), the metal surface is protected by the coating film.

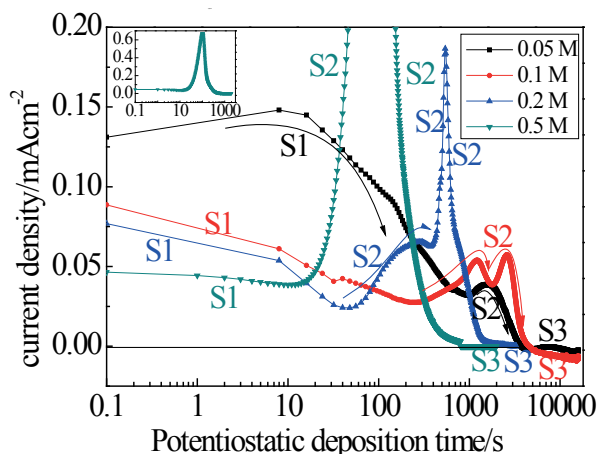


**Figure 1:** Current decay for depositing fluoride conversion film on AZ31 Mg alloy at  $-1.4$  V in 0.05 M, 0.1 M, 0.2 M and 0.5 M deaerated KF solutions with pH 7.5 at room temperature.

In S1 stage, as a potential is applied onto the AZ31 Mg alloy, the plate condenser formed between the AZ31 Mg alloy and KF solution is charged instantly, and electrode reactions occur simultaneously. With prolonging time, the charging current decreases, meanwhile, the faraday current increases. As shown in stage 1, when the decrease of the charging current is larger than the increase of the faraday current, the total current drops with time. With increasing the KF concentration, the charging current decreases and the charging time shortens. The decrease of the charging current can be ascribed to the decrease of the capacitance of the electric double layer between electronic conductor (AZ31 Mg alloy) and ionic conductor (KF electrolyte solution), and the decrease of capacitance is caused by the precipitate of fluoride. It is believed that increasing the concentration of KF can promote the formation of fluoride precipitate on AZ31 magnesium alloy. In addition, the shortening of charging time is caused by the decrease of both capacitance and the solution resistance. Normally, the solution resistance decreases with increasing the concentration of KF.

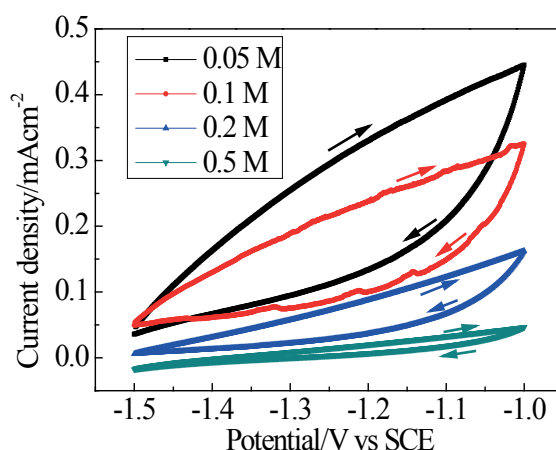
S2 Stage as presented in Figure 1 shows that the total current increases with time when the increase of the faraday current is larger than the decrease of the charging current. The increase of the faraday current density suggests that the corrosion products cannot resist the dissolution of AZ31 Mg alloy substrate. Instead, the drop of the current density corresponds to the formation of a corrosion resistant component in the coating process. However, with an increase in the concentration of KF, the coating time shortens while the peak current density enlarges. In 0.05 M KF solution, only one current peak that locates in the time range of 1040 s~3700 s is observed, and the current density first increases from  $32.2 \mu\text{A}/\text{cm}^2$  to  $38.5 \mu\text{A}/\text{cm}^2$ , then it drops to about zero. However, as mentioned in the reference<sup>[30]</sup>, two current peaks that locate in the time range of 250 s~4660 s are observed in 0.1 M KF solution. The first peak (1200 s,  $54 \mu\text{A}/\text{cm}^2$ ) was ascribed to the chemical conversion process of non-protective  $\text{Mg}(\text{OH})_2$  to  $\text{MgF}_2$ , and the second peak (2700 s,  $57 \mu\text{A}/\text{cm}^2$ ) was caused by the deposition of a stable protective film composed of  $\text{Mg}(\text{OH})_2$ ,  $\text{MgF}_2$  and  $\text{KMgF}_3$ . The coating process in 0.2 M KF solution is similar to that in 0.1 M KF solution, and two equivalent current peaks that locate in the time range of 48 s~2000 s are observed. However, the coating time in 0.1 M KF solution is far longer than that in 0.2 M KF solution, while the intensity of the two current peaks in 0.1 M KF solution is weaker than that in 0.2 M KF solution. Finally, the coating process in 0.5 M KF solution only shows one current peak in the time range of 20 s~800 s, and the peak current density reaches a maximum of  $670 \mu\text{A}/\text{cm}^2$  at 100 s. Furthermore, the peak area integral of the current decay plot may represent the faraday transfer charge during the coating process. The integral results show that the faraday charges corresponding to 0.05 M, 0.1 M, 0.2 M and 0.5 M KF solutions are  $116.9 \text{ mCcm}^{-2}$ ,  $154.2 \text{ mCcm}^{-2}$ ,  $78.8 \text{ mCcm}^{-2}$  and  $70 \text{ mCcm}^{-2}$ , respectively. These transferred faraday charges may be correlated with the amount of the electrochemical deposited FCF coating<sup>[31]</sup>.

After the current peak of coating process, the AZ31 Mg alloy substrate is protected by the coating film, and the current density decays to a very low value. The current density changes from positive values to negative values for 0.05 M KF solution at 3728 s and 0.1 M KF solution at 4660 s, which can be attributed to the galvanic effect of the film to the AZ31 Mg substrate<sup>[30]</sup>.

As the galvanized potential gets higher than the applied potential, the AZ31 Mg alloy behaviors as a cathode, thus the current changes to a cathodic current. However, the current densities for 0.2 M and 0.5 M KF solutions keep above zero, which is ascribed to the dense film with high content of fluorine to resist the electrolyte penetration. Additionally, the shape of the current decay curves indicates that the deposition process of the film follows the layer by layer mechanism<sup>[32]</sup>.

### Cyclic voltammetry study of passivation of the Mg alloy surface

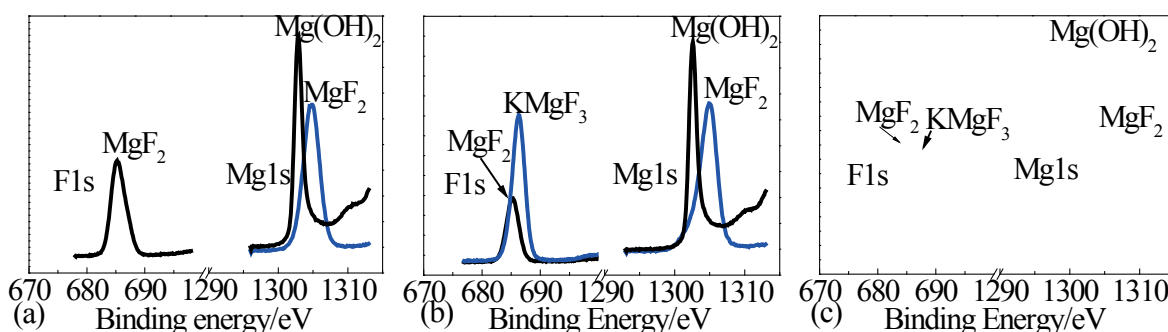
Figure 2 shows the cyclic voltammetry curves of the AZ31 Mg alloy in the solutions of different KF concentrations at pH 7.5. The sweeping potential range is from  $-1.5$  V to  $-1.0$  V, and the scanning rate is 150 mV/s. All of the curves are closed loops. In each curve, the current density increases with the potential sweeping forward while it decreases with the potential sweeping backward. The current density in the backward sweep is lower than that in the forward sweep, which should be caused by the precipitate formed by the reaction between AZ31 Mg alloy and the solution. With increasing the KF concentration, the current densities in both forward and backward sweeps and the area of the closed loops decrease. It indicates that the increase of KF concentration can enhance the protection of the precipitate from the anodic dissolution of AZ31 Mg alloy, conversely, it reduces the amount of the precipitate deposited on the alloy surface. Moreover, as shown in Figure 2, the initial current density corresponding to the starting point also decreases with increasing KF concentration, and the initial current densities in 0.05~0.2 M KF solutions are positive while that in 0.5 M KF solution becomes negative. It demonstrates that the increase of KF concentration can enhance the open circuit potential of AZ31 Mg alloy in the solutions, and the electrode potential in 0.5 M KF solution becomes higher than the applied potential of  $-1.5$  V vs SCE so that the electrode behaves as a cathode. The other three still behave as anodes since the enhanced potentials are lower than the applied potential.



**Figure 2:** Voltammetric response of AZ31 Mg alloy immersed in different concentrations of deaerated KF solution with pH 7.5 at room temperature.

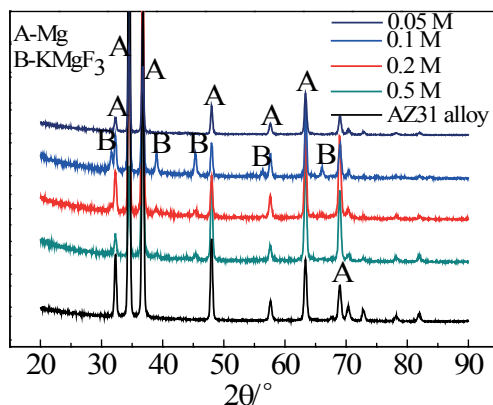
### Analysis of FCF

Figure 3a-c shows the XPS spectra of fluoride film deposited on AZ31 Mg alloy in the deaerated 0.05 M, 0.2 M and 0.5 M KF solutions with pH 7.5 at  $-1.4$  V for 16,000 s, 3000 s and 2000 s, respectively. Another one for 0.1 M KF solution was already shown in reference<sup>[30]</sup>. In these figures, the Mg-1s spectra present two peaks. One corresponds to  $\text{MgF}_2$  (Binding energy, BE = 1304.95 eV), and the other corresponds to Mg hydroxide,  $\text{Mg}(\text{OH})_2$  (BE = 1302.7 eV). The peak corresponding to F-1s spectra shown in Figure 3a can be assigned to  $\text{MgF}_2$  (BE = 685.4 eV). Similar to the Mg-1s spectra, the F-1s spectra shown in Figure 3b-c also show two peaks. One is assigned to  $\text{MgF}_2$  (BE = 685.4 eV), and the other is assigned to  $\text{KMgF}_3$  (BE = 686.5 eV). Thus, it indicates that the film formed in 0.05 M KF solution is composed of  $\text{Mg}(\text{OH})_2$  and  $\text{MgF}_2$ <sup>[33]</sup>, while the films formed in the other three solutions are composed of  $\text{Mg}(\text{OH})_2$ ,  $\text{MgF}_2$  and  $\text{KMgF}_3$ .



**Figure 3:** High-resolution XPS spectra of Mg-1s and F-1s in the film obtained at  $-1.4$  V in different concentrations of deaerated KF solutions with pH 7.5 at room temperature for different time: (a) 0.05 M, 16000 s (b) 0.2 M, 3000 s (c) 0.5 M, 2000 s.

Figure 4 displays the XRD patterns of the fluoride film deposited on AZ31 Mg alloy in 0.05 M, 0.1 M, 0.2 M and 0.5 M KF solutions with pH 7.5 at  $-1.4$  V for 16,000 s, 16,000 s, 3000 s and 2000 s, successively. It confirms that the  $\text{KMgF}_3$  phase exists in the film formed in 0.1 M, 0.2 M and 0.5 M KF solutions but the absence of  $\text{KMgF}_3$  phase in the film deposited in 0.05 M KF solution. However, as shown in Figure 4,  $\text{Mg}(\text{OH})_2$  and  $\text{MgF}_2$  are not detected by the XRD examination, which indicates that these two phases may be amorphous. This agrees well with the results obtained by Pereda et al. [27]. Moreover, as KF concentration increases from 0.1 M to 0.5 M, the diffraction peaks of  $\text{KMgF}_3$  broaden and weaken, meaning a decrease in the crystallinity of  $\text{KMgF}_3$ .



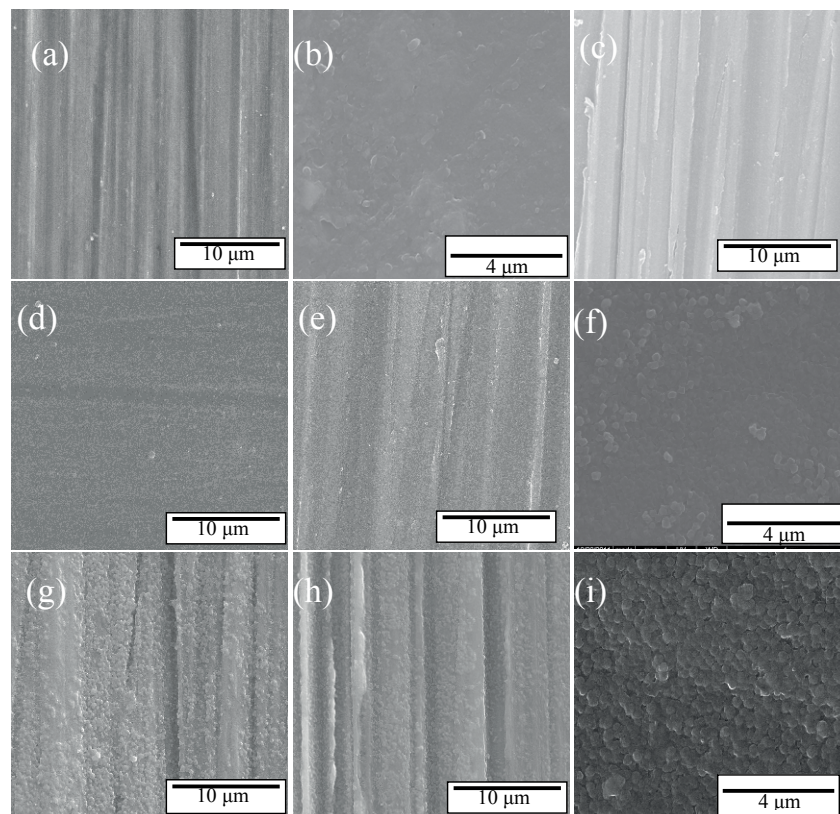
**Figure 4:** X-ray diffraction patterns of untreated AZ31 alloy and AZ31 alloy after polarization at  $-1.4$  V at room temperature in deaerated 0.05 M, 0.1 M, 0.2 M and 0.5 M KF solutions with pH 7.5 for 16,000 s, 16,000 s, 3000 s and 2000 s, respectively.

**Table 1:** The chemical composition of corresponding polarized surfaces.

C <sub>KF</sub> element	0.05 M		0.2 M				0.5 M		
	1664 s	16000 s	300 s	380 s	544 s	3000 s	10 s	100 s	2000 s
O	√	√	√	√	√	√	√	√	√
Mg	√	√	√	√	√	√	√	√	√
F		√		√	√	√	√	√	√
K						√			√

Figure 5a-i shows the surface morphologies of AZ31 Mg alloy after the potentiostatic polarization at  $-1.4$  V in deaerated KF solutions with pH 7.5, among which Figure 5a and b correspond to the polarization time of 1664 s and 16,000 s in 0.05 M, Figure 5c-f to 300 s, 380 s, 544 s and 3,000 s in 0.2 M, and Figure 5g-i to 10 s, 100 s and 2,000 s for 0.5 M, successively. Table 1 exhibits the elemental composition derived from EDS spectra of the respective polarized surfaces. It is necessary to point out that the morphologies and EDS plots for 0.1 M KF solution was also reported in reference [30]. In Figure 5a, the abrasive marks of the sand paper are still observable on the substrate surface, and Table 1 indicates that the polarized surface is composed of Mg and O, which means  $\text{OH}^-$  or/and  $\text{O}^{2-}$  has combined with the Mg substrate in the first stage of the current decay. In Figure 5b, the surface is rough and the abrasive marks of the sand paper are filled and leveled up by the precipitates, indicating the deposition of a film on the specimen surface. Table 1 reveals that the film is composed of Mg, F and O, suggesting that F ions have participated in forming a coating film. When AZ31 Mg alloy was polarized in 0.2 M KF solution for 300 s as shown in Figure 5c, the abrasive marks of the sand paper are still observable on the substrate surface, and Table 1 indicates that the polarized surface is composed of Mg and O, which means  $\text{OH}^-$  or/and  $\text{O}^{2-}$  has combined with the Mg substrate in the first stage of the current decay. As the polarization continued to 380 s, a smooth coating morphology was revealed (see Figure 5d), and the Mg, F and O elements are detected, indicating F ions have participated in the formation of the conversion film. However, the morphology presented in Figure 5e does not show big difference from that shown in Figure 5d, and the chemical composition of the polarized surface shown in Figure 5e is the same with that shown in Figure 5d, which means  $\text{MgF}_2$  may be transformed to  $\text{Mg}(\text{OH})_2$ , leading to a deterioration of the protectiveness of  $\text{MgF}_2$  and inducing a current increase from 380 s to 544 s in the current decay curve. Furthermore, as the polarization continued to 3000 s, as shown in Figure 5f, the surface morphology reveals a coating layer composed of crystallized particles. The elemental composition of the corresponding surface indicates that the polarized surface is composed of Mg, F, O and K, indicating  $\text{K}^+$  ions have participated in the formation of the conversion film in the final of the current decay. According to the XRD database and the Refs [27] and [30], the crystallized particles can be identified as  $\text{KMgF}_3$ . Figure 5g and 5h reveals the surface morphologies of AZ31 Mg alloy polarized for 10 s and 100 s in 0.5 M KF solution, respectively. Comparisons of Figure 5g with 5h and the element composition of these two polarized surfaces show the very similar abrasive marks of the sand paper in the morphology and the same elemental composition of O, Mg and F, which indicates that  $\text{Mg}(\text{OH})_2$  film is already transformed to  $\text{MgF}_2$  film within 10 s, but  $\text{KMgF}_3$  particles start to crystallize until 100 s. It is different from the morphology shown in Figure 5a, 5g, 5h show some new scales upon the coating surface with the abrasive marks of the sand paper, which can be ascribed to be that the increase of KF concentration promote the conversion rate of  $\text{Mg}(\text{OH})_2$  to  $\text{MgF}_2$  (see formula (1)). As the polarization continued to 2000 s, the surface morphology reveals a coating layer consisting of crystallized particles, as shown in Figure 5i, and Table 1 indicates that the polarized surface is composed of Mg, F, O and K, indicating  $\text{K}^+$  ions have participated in the formation of the

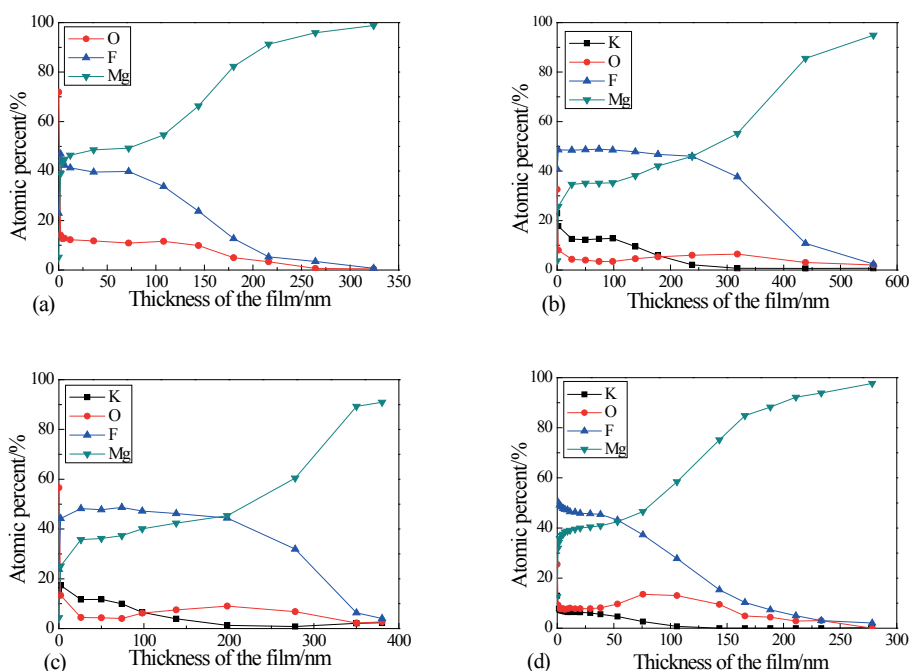
conversion film from 100 s to 2000 s in the current decay. Based on the XRD examination and the results in Refs [27] and [30], the crystallized particles can be identified as  $\text{KMgF}_3$ . However, it is necessary to point out that  $\text{KMgF}_3$  was detected at the end of the polarization in 0.1 M~0.5 M KF solutions, and after that the coating film becomes a stable protective layer. The variation of the surface morphologies is indicative of the variation of the chemical composition of the film [28]. A comparison of Figure 5b, 5f and 5i with the surface morphology of the AZ31 Mg alloy polarized in 0.1 M KF solution for 16000 s [30] shows that  $\text{KMgF}_3$  deposited in 0.1 M KF solution has the greatest size and optimal crystallinity, nevertheless, increasing the KF concentration causes a decrease in the size and crystallinity of  $\text{KMgF}_3$  and decreasing the KF concentration results in no formation of  $\text{KMgF}_3$ . These results are consistent with the XRD analysis. According to the crystal growth theory [35], the crystal growth process includes two stages, i. e. the nucleus formation and followed by the crystal growth. If KF solution is limited at a low concentration (0.05 M), the nucleus cannot form, and thus few crystals are formed, as shown in Figure 5b. As the KF concentration increases to 0.1 M, the rate of the nucleus formation ( $R_{nf}$ ) is lower than the rate of the crystal growth ( $R_{cg}$ ), the nucleus has enough time (see Figure 1) to grow into a complete crystal, and thus the formed crystals have the greatest size and complete shape. However, further increasing KF concentration can cause  $R_{nf} > R_{cg}$ , which means that the previous formed nucleus cannot grow into the complete crystal before the new nucleus forms. Thus, the formed crystals have smaller size and more incomplete shape (see Figure 5f and 5i).



**Figure 5:** The surface morphologies micrographs and corresponding EDS plots of specimens polarized at -1.4 V at room temperature in different concentrations of deaerated KF solutions with pH 7.5 for different time: (a) 0.05 M, 1664 s (b) 0.05 M, 16000 s (c) 0.2 M, 300 s (d) 0.2 M, 380 s (e) 0.2 M, 544 s (f) 0.2 M, 3000 s (g) 0.5 M, 10 s (h) 0.5 M, 100 s (i) 0.5 M, 2000 s.

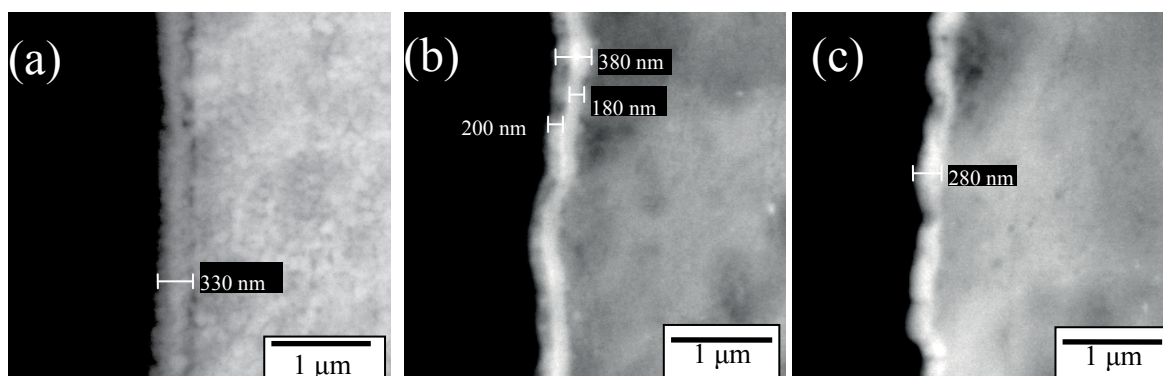
Figure 6a-d exhibits the elemental depth profiles of the specimen surface after polarization at -1.4 V in the deaerated 0.05 M, 0.1 M [30], 0.2 M and 0.5 M KF solutions with pH 7.5 for 16000 s, 16000 s, 3000 s and 2000 s, respectively. Figure 6a indicates that from 330 nm depth (substrate) to the origin (the film surface), the atomic percent of F gradually increases from a trace level to 45%, meanwhile, that of Mg decreases from 99% to 45%, and that of O increases from trace levels to 11%. Figure 6c indicates that the atomic percent of F gradually increases from trace levels at 380 nm depth (substrate) to 49% at the origin (the film surface), meanwhile, that of Mg gradually decreases from 91% to 25%, and that of O experiences a small fluctuation throughout the film. Moreover, K is detected at 200 nm depth, then it gradually increases to about 11.6% at 50 nm depth, and finally it keeps 11.6% constant till the origin (the film surface). Figure 6d reveals that F is detected at 280 nm depth (substrate), then it increases to 49% at 40 nm depth, and finally it keeps 49% constant till the origin (the film surface). Simultaneously, Mg gradually decreases from 98% at 280 nm to 25% at the origin, and O also experiences a small fluctuation throughout the film. However, K is detected at 125 nm depth, then it gradually increases to about 8% at 25 nm depth, and finally it keeps 8% constant till the origin. The fluctuations of the atomic percent of all elements along the thickening of the film indicates that the film deposited in 0.05 M KF solution is comprised of a monolayer with the thickness of 330 nm and composition of O, Mg and F elements. The films deposited in 0.2 M and 0.5 M KF solution, which are similar to that formed in 0.1 M KF solution, contain an inner layer with the composition of O, Mg and F elements and the thickness of 180 nm and 155 nm, respectively. While the out layers deposited in 0.2 M and 0.5 M KF solution consists of O, Mg, K and F elements and have the thickness of 200 nm and 125 nm, respectively.

Figure 7a-c shows the cross-section SEM images of the specimens polarized at  $-1.4$  V in deaerated 0.05 M, 0.2 M and 0.5 M KF solution with pH 7.5 for 16000 s, 3000 s and 2000 s, respectively. Figure 7a indicates that the film is composed of one monolayer with the thickness of 330 nm. While Figure 7b shows that the film is composed of an inner layer with the thickness of 180 nm and an outer layer with the thickness of 200 nm, which is similar to that formed in 0.1 M KF solution<sup>[30]</sup>. However, Figure 7c apparently reveals that the film comprises a monolayer with the thickness of 280 nm. According to Figure 6c, this monolayer can be divided into an inner layer with the thickness of 155 nm and an outer layer with the thickness of 125 nm. Obviously, the film thickness estimated with SEM is consistent with that estimated with XPS. Comparing the cross-section SEM images of the FCF coatings shown in Figure 7a-c with that obtained at  $-1.4$  V in 0.1 M KF solution for 16000 s<sup>[30]</sup> indicates that the thickness of the film decreases with increasing the concentration of KF from 0.1 M to 0.5 M, but it is out of the ordinary for 0.05 M KF solution since the formed layer is unilaminar. In addition, deposition time for the film deposited in 0.05 M, 0.1 M, 0.2 M and 0.5 M KF solutions is successively 16000 s, 16000 s, 3000 s and 2000 s. According to the micro-structure of these layers, the unilaminar layer in 0.05 M consumes 16000 s, while for the double layer, the inner one consumes 2700 s for 0.1 M, 544 s for 0.2 M and 100 s for 0.5 M, and the outer one consumes 13300 s for 0.1 M, 2456 s for 0.2 M and 1900 s for 0.5 M.



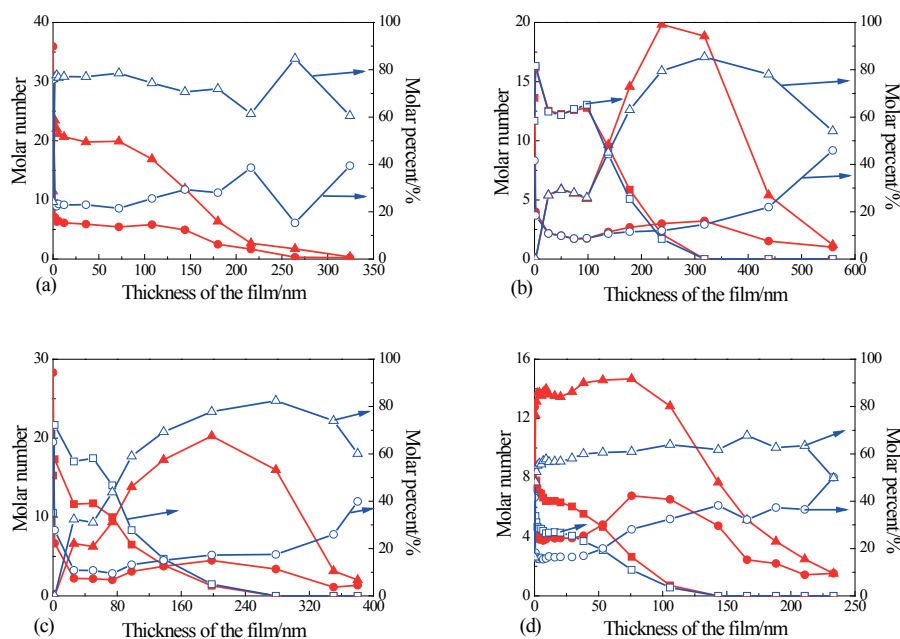
**Figure 6:** XPS elemental depth profiles of specimens polarized at  $-1.4$  V in different concentrations of deaerated KF solutions with pH 7.5 at room temperature for different time: (a) 0.05 M, 16000 s (b) 0.1 M, 16000 s (c) 0.2 M, 3000 s (d) 0.5 M, 2000 s.

Figure 3 has shown that the film formed in 0.05 M KF solution is composed of  $\text{Mg}(\text{OH})_2$  and  $\text{MgF}_2$ , while those of formed in 0.1 M~0.5 M KF solutions are composed of  $\text{Mg}(\text{OH})_2$ ,  $\text{MgF}_2$  and  $\text{KMgF}_3$ . Thus, according to the calculation method of the molar numbers of  $\text{Mg}(\text{OH})_2$ ,  $\text{MgF}_2$  and  $\text{KMgF}_3$  mentioned in the reference<sup>[30]</sup>, it can semi-quantitatively calculate that their molar numbers. Moreover, some of the residual Mg element can still distribute in the inner layer of FCF close to the Mg matrix, and its atomic percent (also the residual atomic number) should equal to the atomic percent difference between the total atomic percent of Mg and the sum of those transformed into the FCF. Thus, the total molar number of all substances in the FCF should equal to the sum of the molar numbers of  $\text{Mg}(\text{OH})_2$ ,  $\text{MgF}_2$ ,  $\text{KMgF}_3$  and the residual Mg. However, the molar percent of  $\text{Mg}(\text{OH})_2$ ,  $\text{MgF}_2$ ,  $\text{KMgF}_3$  are assumed as the quotient between the molar number of each constitute and the sum of the molar numbers of  $\text{Mg}(\text{OH})_2$ ,  $\text{MgF}_2$ ,  $\text{KMgF}_3$ . Accordingly, it can calculate the depth profiles of each constitute in the FCF.



**Figure 7:** Cross-section SEM images of specimens polarized at  $-1.4$  V in different concentrations of deaerated KF solutions with pH 7.5 at room temperature for different time: (a) 0.05 M, 16000 s (b) 0.2 M, 3000 s (c) 0.5 M, 2000 s.

Figure 8a-d shows the depth profiles of  $\text{Mg}(\text{OH})_2$ ,  $\text{MgF}_2$  and  $\text{KMgF}_3$  in the film deposited in 0.05 M, 0.1 M, 0.2 M and 0.5 M KF solutions at  $-1.4$  V for 16 000 s, 16 000 s, 3 000 s and 2 000 s, respectively. The left axis of the ordinates denotes the molar number while the right one denotes the molar percent of the transformed compositions. In 0.05 M KF solution, as shown in Figure 8a, the FCF layer is comprised of  $\text{Mg}(\text{OH})_2$  and  $\text{MgF}_2$ , while  $\text{KMgF}_3$  was not observed. It may be ascribed to be that KF concentration is too low to form  $\text{KMgF}_3$ . The molar numbers of both  $\text{Mg}(\text{OH})_2$  and  $\text{MgF}_2$  are limited at a trace level from 330 nm to 220 nm, then they respectively increase to about 6 and 20 at 70 nm, and finally they respectively maintain 6 and 20 till the origin (the film surface). Moreover, the molar percent of  $\text{MgF}_2$  increases with the decrease of that of  $\text{Mg}(\text{OH})_2$ , which indicates the chemical conversion of  $\text{Mg}(\text{OH})_2$  to  $\text{MgF}_2$ . Figure 8a presents that the molar percent ratio of  $\text{MgF}_2$  to  $\text{Mg}(\text{OH})_2$  in the outside part is close to a constant, which may be caused by the stable conversion process that executes an equilibrium reaction by formula (1). In 0.1 M~0.5 M KF solutions, the FCF layers shown in Figure 8b-d are comprised of  $\text{Mg}(\text{OH})_2$ ,  $\text{MgF}_2$  and  $\text{KMgF}_3$  with the thickness of around 560 nm for 0.1 M, 380 nm for 0.2 M, and 280 nm for 0.5 M.  $\text{Mg}(\text{OH})_2$  and  $\text{MgF}_2$  appear throughout the film, their molar numbers along the film thickness show a maximum at 239 nm for 0.1 M, 197 nm for 0.2 M, and 165 nm for 0.5 M. They always simultaneously increase or decrease, and the content of  $\text{MgF}_2$  is always higher than that of  $\text{Mg}(\text{OH})_2$ . While  $\text{KMgF}_3$  starts to appear in the depth of 320 nm for 0.1 M, 180 nm for 0.2 M, and 140 nm for 0.5 M. From 0.1 M to 0.5 M KF solution, the molar number of  $\text{KMgF}_3$  increases successively from zero at 320 nm, 180 nm and 140 nm to 12.5 at 100 nm, 12 at 50 nm, and 6.5 at 20 nm, then it maintains 12.5, 12 and 6.5 till the thickness of 72 nm, 24.5 nm and 14 nm, and finally it respectively increases to 16.25, 17.5, and 8 at the origin (the film surface). According to the depth profiles of  $\text{Mg}(\text{OH})_2$ ,  $\text{MgF}_2$  and  $\text{KMgF}_3$ , it can be derived that the inner layer is composed of  $\text{Mg}(\text{OH})_2$  and  $\text{MgF}_2$ , while the outer layer consists of  $\text{Mg}(\text{OH})_2$ ,  $\text{MgF}_2$  and  $\text{KMgF}_3$ . In addition, it is necessary to point out that by comparing the molar percent of  $\text{Mg}(\text{OH})_2$ ,  $\text{MgF}_2$  and  $\text{KMgF}_3$  along the film thickness, the molar percent of  $\text{MgF}_2$  increases with the decrease of that of  $\text{Mg}(\text{OH})_2$  in the inner layer, and the molar percent of  $\text{KMgF}_3$  increases with the decrease of that of  $\text{MgF}_2$  in the outer layer, indicating the transformation of  $\text{Mg}(\text{OH})_2$  to  $\text{MgF}_2$  in the inner layer and  $\text{MgF}_2$  to  $\text{KMgF}_3$  in the out layer.



**Figure 8:**  $\text{Mg}(\text{OH})_2$  ( $\bullet$ ○),  $\text{MgF}_2$  ( $\blacktriangle$ □) and  $\text{KMgF}_3$  ( $\blacksquare$ □) depth profiles of specimens polarized at  $-1.4$  V in different concentrations of deaerated KF solutions with pH 7.5 for different time: (a) 0.05 M, 16000 s (b) 0.1 M, 16000 s (c) 0.2 M, 3000 s (d) 0.5 M, 2000 s.

In sum, the potentiostatic deposition process of the conversion film on AZ31 Mg alloy in 0.05 M KF solution executes an equilibrium conversion as described in formula (1), and the molar percent ratio of  $\text{MgF}_2$  to  $\text{Mg}(\text{OH})_2$  is close to a constant as shown in Figure 8a. While in 0.1 M and 0.2 M KF solutions, the crystallization process of  $\text{KMgF}_3$  may execute the reaction of  $\text{MgF}_2$  combining with KF as shown in formula (2). The molar percent of  $\text{KMgF}_3$  increases with the decrease of the molar percent of  $\text{MgF}_2$  while that of  $\text{Mg}(\text{OH})_2$  basically maintains a constant as shown in Figure 8b and 8c. Moreover, in 0.5 M KF solution, the formation process of  $\text{KMgF}_3$  may execute an additional reaction besides formula (2), which can be written as formula (3):



The molar percent of  $\text{KMgF}_3$  increases with decreasing that of  $\text{MgF}_2$  and  $\text{Mg}(\text{OH})_2$ , as shown in Figure 8d.

A Comparison of Figure 8b-8d, it is easy to find that the molar percent of  $\text{KMgF}_3$  decreases with increasing KF concentration. It is probably caused by two reasons. One is that during the formation process of the fluoride conversion film, increasing KF concentration will promote the release of  $\text{OH}^-$  ions by the formula (1) and (3), which may cause the surface passivation of AZ31 Mg alloy substrate. Additionally, the more concentrated F is probably adsorbed on the surface of AZ31 Mg alloy substrate, which may suppress the anodic dissolution of AZ31 Mg alloy, and thus reducing the chemical conversion rate.

Figure 9 shows the Nyquist plots of the anodic potentiostatic polarized specimens in 0.1 M NaCl solution. In general, the plots present two capacitance arcs in the high frequency region and one inductance arc in the low frequency regions. For comparing the corrosion resistance of the polarized specimens, the real impedance ( $Z'$ ) at which the imaginary part ( $Z''$ ) vanishes from the capacitive part can be taken as the charge transfer resistance  $R_t$ , and regard it as a measure of the corrosion resistance [29, 36-37]. It is estimated that  $R_t$  of the polarized specimen is 660  $\Omega\text{cm}^2$  for 0.05 M, 2600  $\Omega\text{cm}^2$  for 0.1 M, 1830  $\Omega\text{cm}^2$  for 0.2 M, and 1300  $\Omega\text{cm}^2$  for 0.5 M. As compared with Figure 8, the corrosion resistance of the polarized specimen should be correlated with the thickness and chemical compositions of the films. Figure 8 indicates that both the content of  $\text{KMgF}_3$  and the thickness of the film decrease with increasing KF concentration from 0.1 M to 0.5 M, which just right corresponds to the decreasing sequence of the corrosion resistance with increasing KF concentration. However, the film deposited in 0.05 M KF solution is 330 nm thick and only composed of  $\text{MgF}_2$  and  $\text{Mg}(\text{OH})_2$  without  $\text{KMgF}_3$ . In addition, Figure 7 also shows that the film formed in 0.05 M KF solution is more porous than those formed in more concentrated KF solutions. It is these reasons that result in lower corrosion resistance of the film formed in 0.05 M KF solution than those of deposited in more concentrated KF solutions. Therefore, the content of  $\text{KMgF}_3$  may play a more important role in enhancing the corrosion resistance, followed by the film thickness.

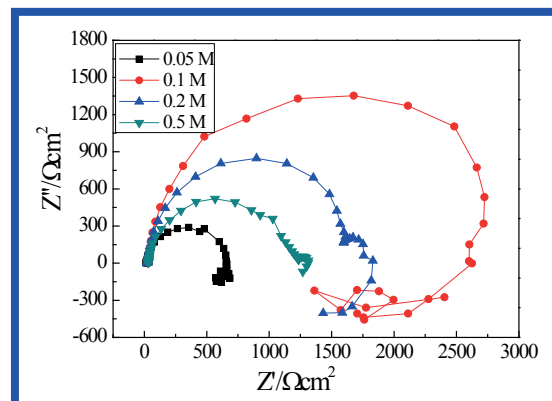


**Figure 9:** Nyquist plots of specimens polarized at  $-1.4$  V at room temperature in deaerated 0.05 M, 0.1 M, 0.2 M and 0.5 M KF solutions with pH 7.5 for 16,000 s, 16,000 s, 3000 s and 2000 s, respectively.

## CONCLUSIONS

As summarized from the above experimental results and discussion, the effect of KF concentration on the potentiostatic deposited film on AZ31 Mg alloy can be concluded as follows:

(1) The concentration of KF determines the film composition, the coating time, the thickness and the corrosion resistance.

(2) The formed film in 0.05 M KF solution is a monolayer composed of amorphous  $\text{Mg}(\text{OH})_2$  and  $\text{MgF}_2$ , while amorphous  $\text{Mg}(\text{OH})_2$  and  $\text{MgF}_2$  and crystallized  $\text{KMgF}_3$  as a double layer in more concentrated KF solutions. The composition of inner layer is the same as that of the monolayer, while the outer layer is composed of amorphous  $\text{Mg}(\text{OH})_2$  and  $\text{MgF}_2$  and crystallized  $\text{KMgF}_3$ . Continually increasing KF concentration reduces the content of  $\text{KMgF}_3$  in the outer layer.

(3) Continually increasing KF concentration shortens the coating duration and reduces the film thickness. The corrosion resistance of the fluoride conversion film is closely correlated with the content of  $\text{KMgF}_3$  and the thickness.

## ACKNOWLEDGEMENTS

This work was financially supported by the National Basic Research Program of China (973 program, grant No. 2012cb619101) and the National Science Fund of China (No. 51131007).

## REFERENCES

1. Guan X, et al. Enhancement of osteogenesis and biodegradation control by brushite coating on Mg–Nd–Zn–Zr alloy for mandibular bone repair. *Appl Mater Interfaces* (2014) 6: 21525–21533.
2. Haude M, et al. Safety and performance of the drug-eluting absorbable metal scaffold (DREAMS) in patients with de-novo coronary lesions: 12 month results of the prospective, multicentre, first-in-man biosolve-I trial. *Lancet*. (2013) 381: 836–844.
3. Srinivasan A, et al. Electrochemical polymerization of pyrrole over AZ31 Mg alloy for biomedical applications. *Electrochimica Acta* (2013) 88: 310–321.
4. Witte F, et al. In vivo corrosion of four magnesium alloys and the associated bone response. *Biomaterials* (2005) 26: 3557–3563.
5. Hornberger H, et al. Biomedical coatings on magnesium alloys—a review. *Acta Biomater* (2012) 8: 2442–2455.

6. Xin Y, et al. Influence of aggressive ions on the degradation behavior of biomedical magnesium alloy in physiological environment. *Acta Biomater* (2008) 4: 2008–2015.
7. Lévesque J, et al. Investigation of corrosion behaviour of magnesium alloy AM60B-F under pseudo-physiological conditions. *Mater Sci Forum* (2003) 521–526.
8. Carboneras M, et al. Biodegradation kinetics of modified magnesium-based materials in cell culture medium. *Corros. Sci* (2011) 53: 1433–1439.
9. Witte F, et al. In vivo corrosion and corrosion protection of magnesium alloy LAE442. *Acta Biomater* (2010) 6: 1792–1799.
10. Turhan MC, et al. Effect of acidic etching and fluoride treatment on corrosion performance in Mg alloy AZ91D (MgAlZn). *Electrochimica Acta* (2009) 55: 250–257.
11. Mao L, et al. Enhanced bioactivity of Mg–Nd–Zn–Zr alloy achieved with nanoscale MgF<sub>2</sub> surface for vascular stent application. *Appl Mater Interfaces* (2015) 7: 5320–5330.
12. Drynda A, et al. Development and biocompatibility of a novel corrodible fluoride-coated magnesium-calcium alloy with improved degradation kinetics and adequate mechanical properties for cardiovascular applications. *J Biomed Mater Res Part A* (2010) 93: 763–775.
13. Li N, et al. Corrosion resistance and cytotoxicity of a MgF<sub>2</sub> coating on biomedical Mg-1Ca alloy via vacuum evaporation deposition method. *Surf Interface Anal* (2013) 45: 1217–1222.
14. Ye XY, et al. The influence of HF treatment on corrosion resistance and in vitro biocompatibility of Mg-Zn-Zr alloy. *Front Mater Sci* (2010) 4: 132–138.
15. Lalk M, et al. Fluoride and calcium-phosphate coated sponges of the magnesium alloy AX30 as bone grafts: a comparative study in rabbits. *J Mater Sci Mater Med* (2012) 24: 417–436.
16. Lellouche J, et al. Antibiofilm activity of nanosized magnesium fluoride. *Biomaterials* (2009) 30: 5969–5978.
17. Lellouche J, et al. Improved antibacterial and antibiofilm activity of magnesium fluoride nanoparticles obtained by water-based ultrasound chemistry. *Nanomedicine* (2012) 8: 702–711.
18. Lellouche J, et al. Antibiofilm surface functionalization of catheters by magnesium fluoride nanoparticles. *Int J Nanomedicine* (2012) 7: 1175–1188.
19. Grillo CA, et al. Biological effects of magnesium particles degradation on UMR-106 cell line: influence of fluoride treatments. *Colloids Surf B: Biointerfaces* (2011) 88: 471–476.
20. Yamamoto A, et al. Surface modification on magnesium alloys by coating with magnesium fluorides. *Mater Sci Forum* (2005) 475–479: 505–508.
21. Seitz JM, et al. Comparison of the corrosion behavior of coated and uncoated magnesium alloys in an in vitro corrosion environment. *Adv Eng Mater* (2011) 13: B313–B323.
22. Ono S and Masuko N. Anodic films growth on magnesium and magnesium alloys in fluoride solutions. *Mater Sci Forum* (2003) 897: 419–422.
23. Ohse T, et al. Surface modification on magnesium alloys by coating with magnesium fluorides. *Mater Sci Forum* (2005) 475–479: 505–508.
24. Thomann M, et al. Influence of a magnesium-fluoride coating of magnesium-based implants (MgCa0.8) on degradation in a rabbit model. *J Biomed Mater Res Part A* (2010) 93: 1609–1619.
25. Carboneras M, et al. Chemical conversion treatments to protect biodegradable magnesium in applications as temporary implants for bone repair. *Rev Metall* (2010) 46: 86–92.
26. Pereda MD, et al. Comparative study of fluoride conversion coatings formed on biodegradable powder metallurgy Mg: the effect of chlorides at physiological level. *Mater Sci Eng C* (2011) 31: 858–865.
27. Pereda MD, et al. Corrosion inhibition of powder metallurgy Mg by fluoride treatments. *Acta Biomater* (2010) 6: 1772–1782.
28. Sankara Narayanan TSN, et al. Tailoring the composition of fluoride conversion coatings to achieve better corrosion protection of magnesium for biomedical applications. *J Mater Chem B* (2014) 2: 3365–3382.
29. Chiu KY, et al. Characterization and corrosion studies of fluoride conversion coating on degradable Mg implants. *Surf Coat Technol* (2007) 202: 590–598.
30. Wu LP, et al. Potentiostatic deposition process of fluoride conversion film on AZ31 magnesium alloy in 0.1 M KF solution. *Electrochim Acta* (2013) 105: 554–559.
31. Efthimiadis J, et al. Potentiostatic control of ionic liquid surface film formation on ZE41 magnesium alloy. *Appl Mater*

Interfaces (2010) 2: 1317–1323.

32. Grubač Z and Hukovic S. Electrodeposition of thin sulfide films: nucleation and growth observed for Bi<sub>2</sub>S<sub>3</sub>, Thin Solid Films (2002) 413: 248–256.
33. Bradford PM, et al. Ion beam analysis of corrosion films on a high magnesium alloy (Magneox Al 80). Corros Sci (1976) 16: 747–766.
34. Tsyntsaru N, et al Structural, magnetic, and mechanical properties of electrodeposited cobalt–tungsten alloys: intrinsic and extrinsic interdependencies. Electrochim Acta (2013) 104: 94–103.
35. Kirkpatrick RJ. Crystal growth from the melt: a review. Am Mineral (1975) 60: 798–814.
36. Lin BL, et al. Effect of molybdate post-sealing on the corrosion resistance of zinc phosphate coatings on hot-dip galvanized steel. Corros Sci (2008) 50: 962–967.
37. Yu BL, et al. Enhancement of corrosion resistance of Mg-9 wt.% Al-1 wt.% Zn alloy by a calcite (CaCO<sub>3</sub>) conversion hard coating. Corros Sci (2010) 52: 1874–1878.